Chinese Chemical Letters 34 (2023) 107887

Contents lists available at ScienceDirect

Chinese Chemical Letters

journal homepage: www.elsevier.com/locate/cclet

Chemoproteomics identifies Ykt6 as the direct target of schisandrin A for neuroprotection

Tiantian Wang, Yu Zhou, Hao Zheng, Tao Shen, Dongmei Wang*, Jinlan Zhang*

State Key Laboratory of Bioactive Substances and Functions of Natural Medicines, Institute of Materia Medica, Chinese Academy of Medical Sciences and Peking Union Medical College, Beijing 100050, China

ARTICLE INFO

Article history:
Received 2 August 2022
Revised 2 October 2022
Accepted 4 October 2022
Available online 9 October 2022

Keywords:
Schisandrin A
Activity-based protein profiling (ABPP)
Neuroprotection
Ykt6
Autophagy

ABSTRACT

Schisandrin A is a natural dibenzocyclooctene lignan with potent neuroprotective activity. However, the specific mechanisms or direct target proteins have not been clarified up to now. In this study, we designed and synthesized the probes of schisandrin A with photoreactive diazirine and clickable alkyne to identify its direct target in SH-SY5Y cells by employing activity-based protein profiling (ABPP) technique. Ykt6 was prominent among the 13 proteins obtained with high confidence and we confirmed Ykt6 as the direct target of schisandrin A by CETSA, IF, SPR and knockdown assay. Functionally, schisandrin A protected the cells against the injury induced by glutamate by regulating autophagy *via* Ykt6. This discovery may provide a novel therapeutic option for various neuronal cell damage-mediated diseases.

Schisandrin A (Sch A), also known as deoxyschisandrin, is a natural dibenzocyclooctene lignan isolated from the fruit of *Schisandra chinensis* (Turcz.) Baill (*S. chinensis*) which has long been used in traditional Chinese medicine to treat spontaneous sweating, chronic asthma, insomnia and amnesia [1,2]. Sch A has multiple pharmacological properties, such as anti-cancer, anti-oxidant, neuroprotective, hepatoprotective, anti-inflammatory activities [1–4]. Recently, it is worth noting that Sch A showed protective effects against various neuronal cell damage-mediated diseases including Cerebral ischemia, Alzheimer's disease, Parkinson's disease and other neurodegenerative diseases [5–7]. Researcher Kim found that Sch A may possess therapeutic potential against neurotoxicity induced by glutamate in primary cortical neurons and the mechanism involved the improvement of the glutathione defense system [8]. Another research indicated that Sch A protected dopaminergic neurons and exerted a neuroprotective effect by enhancing the expression of LC3-II, beclin1, parkin and PINK1 in MPTP-induced mouse model of Parkinson's disease [6]. However, the mechanism of the neuroprotection of Sch A remains inconclusive even after decades of uninterrupted research.

Up to date, the potential targets of Sch A have not been discovered completely due to its multiple pharmacological effects by a variety of biotechnologies, including heat shock factor 1 (HSF1) for colorectal cancer (CRC), pregnane X receptor (PXR) for intrahepatic cholestasis, C5a anaphylatoxin chemotactic receptor (C5aR) for brain ischemia, and arachidonic acid 5-lipoxygenase (ALOX5) for cancer [9–12]. These identified possible targets were not directly related to the mechanism of Sch A against neurotoxicity. It is possible that Sch A might have many other key targets due to the multitargeting profile of natural products. To address these questions, an activity-based protein profiling (ABPP) strategy was applied to perform protein–Sch A interactions [13,14].

In the current work, we designed and synthesized multiple activity-based probes (ABPs) with photoreactive diazirine and clickable alkyne. Then, we utilized probes combined with quantitative chemoproteomic profiling to uncover synaptobrevin homolog YKT6 (Ykt6), a soluble *N*-ethylmaleimide sensitive factor activating protein receptor (SNARE), as the direct target of Sch A. In spite of neurological insults being diverse in nature, the cell injury has collective mechanisms, glutamate-induced neurotoxicity plays a critical role in various neurobiology of disorders such as Parkinson's disease, Alzheimer's disease, epilepsy ischemic stroke, anxiety, and depression [15,16]. Thus, excessive glutamate was used in SH-SY5Y cells to cause neuronal damage and investigated the relation among Sch A, Ykt6 and neuroprotection.

The structure-activity relationship (SAR) of Sch A has been well-established. Firstly, the 1,2,3-trimethoxy moiety attached to the aromatic ring A is vital for the activity, but the 12,13,14-trimethoxy moiety shows no significant effect [15]. Moreover, the nonpolar and bulky substitute at C-14 will improve the activity [15]. Secondly, the contribution of the 7-hydroxy group to the activity has not been confirmed [17–22]. Thirdly, the axial chirality of the

* Corresponding authors.
E-mail addresses: wangdmchina@imm.ac.cn (D. Wang), zhjl@imm.ac.cn (J. Zhang).

https://doi.org/10.1016/j.cclet.2022.107887
1001-8417/

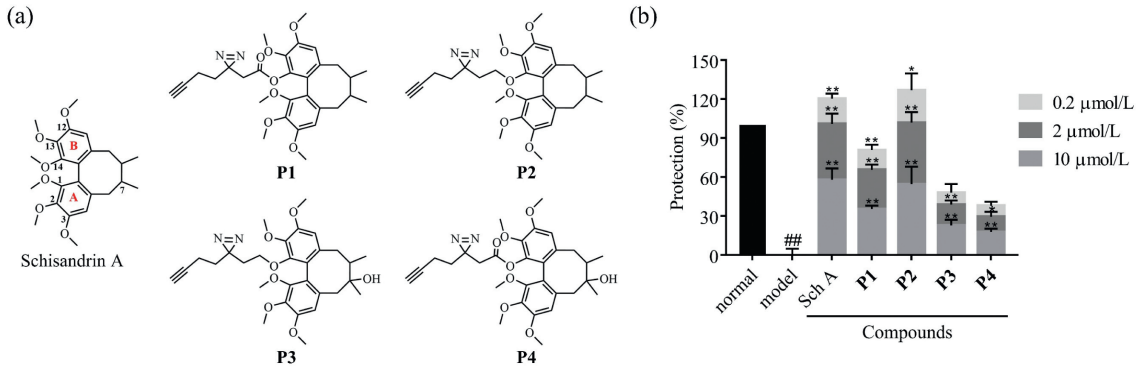

Fig. 1. Chemical structure and the neuroprotective activity evaluation of Sch A and probes. (a) Chemical structures of Sch A and designed probes. (b) The evaluation of the neuroprotective activity of Sch A and designed probes. Data are presented as mean ± SEM, $n = 6$ biological replicates per group. Compared with normal group: $^{\#\#}P < 0.01$; compared with model group: $^{*}P < 0.05$, $^{**}P < 0.01$.

skeleton of dibenzocyclooctadiene lignan does not affect the activity significantly [17,18]. Based on these findings, we were inspired to append a diazirine group and a terminal alkyne handle through the ester or ether bond linking to the 14-position of Sch A to obtain probes **P1** and **P2** (Fig. 1a). Diazirine is a photoreactive group binding proteins stably, and its minimal volume has little effect on the activity of the parent compound. Alkyne allows for highly selective conjugation with reporter groups such as azide-containing fluorescent moieties and biotin by click chemistry [23]. Furthermore, probes **P3** and **P4** with the hydroxy moiety in the 7-position of Sch A were designed to explore the contribution of this hydroxy group to the activity (Fig. 1a). All probes were synthesized based on reported methods and fully characterized by NMR and HRMS before utilized in the subsequent biological evaluations (Supporting information).

With the probes in hand, utilizing the CCK8 assay, we evaluated the neuroprotective activity of Sch A and probes in SH-SY5Y cells induced by glutamate after confirming their cytotoxicity (Fig. S1 in Supporting information). The data showed that **P2** exhibited a similar neuroprotective property to Sch A, while other probes had no significant activities (Fig. 1b). Due to the decrease of polarity, **P2** with the ether linkage performed better neuroprotective activity in SH-SY5Y cells than **P1** with the ester bond. **P3** and **P4** exhibited poor activities, which demonstrated that the 7-hydroxy group negatively regulated the activity of neuroprotection. Therefore, **P2** was taken forward to the target identification investigation. We next examined whether **P2** could label proteins efficiently and specifically *in situ*. The optimal dose, incubation time and UV duration time were initially evaluated. SH-SY5Y cells were incubated with **P2**, then exposed to UV light to facilitate photoaffinity labeling. After that, the cells were lysed and the extracted probe-labeled proteins were cross-linked with TRMRA-azide, then separated by SDS-PAGE and visualized. As shown in Fig. 2a, **P2** was capable of labeling proteins in a concentration-dependent manner. At 10 μmol/L, the fluorescence bands exhibited an excellent intensity of labeling by **P2**. Further, we optimized incubation time and UV irradiation time, and it revealed that cells incubated with **P2** for 1 h and irradiated by UV for 20 min achieved ideal labeling effects (Figs. 2b and c).

With the suitable incubation conditions, we conducted the competition experiment using an in-gel fluorescence assay and bioimaging assay simultaneously to test the accuracy of labeling target proteins. As described in Fig. 2d, it was observed that **P2** labeling was markedly decreased with preincubation of the excess Sch A in a dose-dependent manner, suggesting **P2** bound to the same target proteins as Sch A and the particular protein bands which were blocked dose-dependently by excessive Sch A may contain potential targets of Sch A. Moreover, the result was also supported by the bioimaging studies (Fig. S2 in Supporting information). Although Sch A can be excited with inherent fluorescence at 256 nm [24], it did not interfere with fluorescence microscopy experiments (Fig. S3 in Supporting information). Collectively, the **P2** was proved to be a suitable probe for "target fishing" and the fluorescence intensity of **P2**-labelled proteins on SDS-PAGE served as a convenient read-out for **P2** binding activity.

Given the results above, we performed the pull-down experiment in SH-SY5Y cells to identify the covalent binding targets of **P2**. In order to eliminate false-positive targets, three experiment groups consisting of the negative control group, probe group, and competition group were set. Also, the pull-down experiment was replicated three times to meet statistical demand and the enrichment efficiency of streptavidin beads was confirmed by silver staining (Fig. S4 in Supporting information). Probe-labeled proteins in each group were enriched by biotin-streptavidin beads, then trypsin cleaved and analyzed by nano LC-MS/MS, respectively followed by label-free quantification (workflow, Fig. S5 in Supporting information). Upon obtaining the mass analysis data (Table S1 in Supporting information), we set fold change ≥2, the number of unique peptides ≥4, and the *P*-value ≤0.05 as a standard to screen specific binding proteins. As a result, 171 potential interacting proteins were identified from the probe/negative control group, and 14 proteins were identified from the probe/competition group (Figs. 2e and f). After taking the intersection of these two protein datasets, 13 high-confidence proteins were obtained (Fig. 2g and Table S2 in Supporting information). Cellular localization analysis revealed the main enriched compartments, the endoplasmic reticulum and transport vesicle (Fig. S6 in Supporting information), suggesting that the potential targets may involve vesicle trafficking and membrane fusion. Considering the fold change and subcellular location of these reliable proteins, Ykt6 stood out.

Whether Ykt6 was a direct target of Sch A, further validations were desired. Firstly, a competitive pull-down/western blotting experiment was performed. As expected, Ykt6 was successfully pulled down by **P2** and the labeling decreased dose-dependently in the presence of excess Sch A, which indirectly proved that Sch A interacted with Ykt6 (Fig. 3a). Furthermore, the interaction was also corroborated by the immunofluorescence (IF) experiment. Both the red fluorescence signal generated by **P2**-linked TAMRA and the green signal from Ykt6 localized in the cytoplasm and superimposed well (Fig. 3b), which was consistent with the subcellular location of Ykt6 and showed that Ykt6 was the potential target of Sch A. Besides, a cellular thermal shift assay (CETSA) was performed to validate the direct binding of Ykt6 and Sch A. The ther-

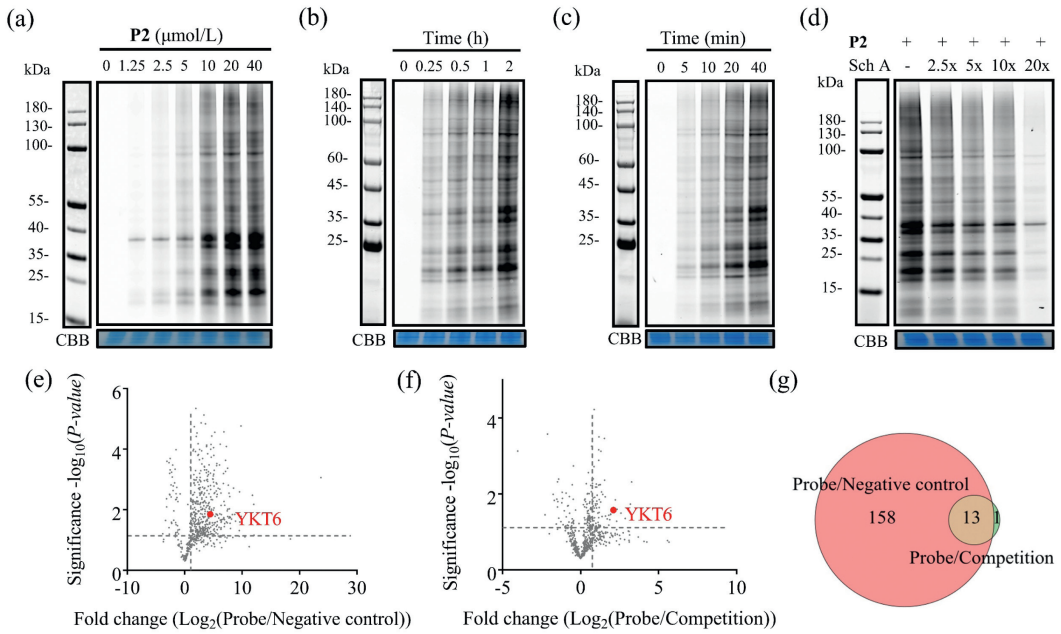

Fig. 2. Evaluation of the labeling efficiency of probe **P2** and target identification of Sch A in living SH-SY5Y cells. Photoaffinity labeling of potential targets in SH-SY5Y cells with probe **P2** in various concentrations (a), incubation time (b) and UV light irradiation time (c). CBB = Coomassie staining. (d) Competitive photoaffinity labeling of potential targets in SH-SY5Y cells with probe **P2** (10 μmol/L) and excessive Sch A. Volcano plot of enriched proteins in the probe/negative control group (e) or in the probe/competition group (f). Ykt6 is highlighted in red, $n = 3$ independent experiments per group. (g) Venn diagram showing the number of proteins that were significantly enriched in both pull-down experiments.

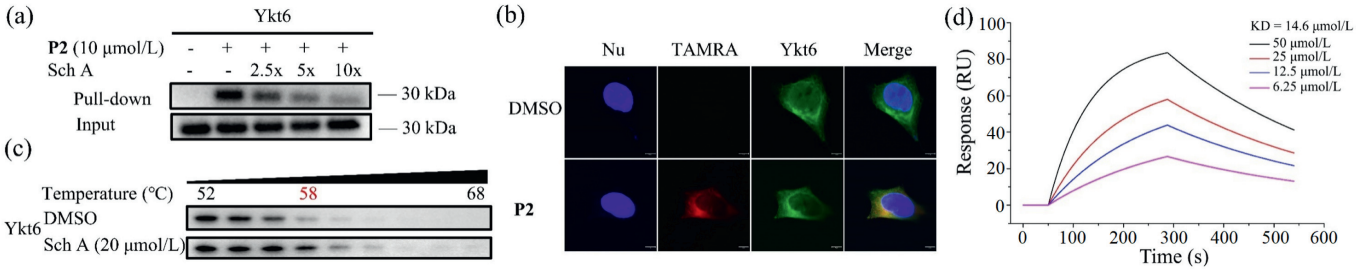

Fig. 3. Validation of interaction between Ykt6 and Sch A. (a) Pull-down/Western blotting was used to validate the Ykt6 with probe **P2** and Sch A. (b) IF confocal imaging of SH-SY5Y cells with **P2**. Immunofluorescence (IF) staining using anti-Ykt6 antibodies. Scale bar = 5 μm. Tetramethylrhodamine = TAMRA. (c) Detection of the interaction between Ykt6 and Sch A by SPR. (d) Evaluation of the thermal stability of Ykt6 incubated with Sch A by CETSA. 58 °C was the critical temperature of protein thermal denaturation.

mal stability of Ykt6 was obviously enhanced after co-incubation with Sch A (Fig. 3c). Finally, a surface plasmon resonance (SPR) assay was applied for tracking the interactions between Sch A and Ykt6 in real-time dynamic analysis. Excitingly, the results showed a remarkable binding affinity with KD values of 14.6 μmol/L (Fig. 3d). To the best of our knowledge, it was the first discovered small molecule that directly interacted with Ykt6.

Research in the last few years suggested that Ykt6 was one of the SNAREs that were responsible for the positioning and fusion of vesicles and targeting membrane layer in the process of vesicle transport, which played an important role in various stages of autophagy [25–27]. It showed that Ykt6 formed a SNARE complex with SNAP29 and lysosomal STX7 to mediate autophagosome-lysosome fusion, and the loss of Ykt6 would lead to a large-scale accumulation of autophagosomes, thereby blocking autophagy flux [28–30]. A further study indicated that Ykt6 restored lysosomal function or reversed autophagic flux damage to involve in neuroprotection [31,32]. Of interest, previous research showed that Sch A exerted a neuroprotective effect by regulating autophagy [6], then the key question concerns whether Sch A regulated autophagy through Ykt6 to exhibit neuroprotective activity.

With these considerations in mind, we firstly explored the necessity of Ykt6 in the neuroprotective effect of Sch A by Ykt6 knock-down assay. The expression levels of Bcl-2 (apoptosis-related protein b-lymphocytoma-2) and Bax (Bcl-2-related X protein) reflect the degree of apoptosis and profile the cell damage status induced by glutamate. Under normal circumstances, when SH-SY5Y cells were incubated with 80 mmol/L glutamate for 16 h, Bcl-2 was down-regulated while Bax was up-regulated, but the pretreatment of Sch A for 8 h reversed this phenomenon in a dose-dependent manner (Fig. 4a). Subsequently, we transfected siRNA to knock down Ykt6, and it showed only mild signs of insult in cells, which may be due to the loss of Ykt6. Next, preincubate SH-SY5Y cells with Sch A followed by glutamate treatment, Sch A hardly showed protective activity (Fig. 4b). The result demonstrated that Sch A exerted neuroprotective activity mostly depending on Ykt6.

Encouraged by this result, the influence of Sch A on the expression of LC3, a classic marker of autophagy, was investigated by western blotting [33]. Sch A was incubated with cells for 8 h followed by 80 mmo/L glutamate treated for 16 h. The result indicated that Sch A could facilitate the autophagy process (Fig. 4c). However, there are many other factors that affect the accuracy

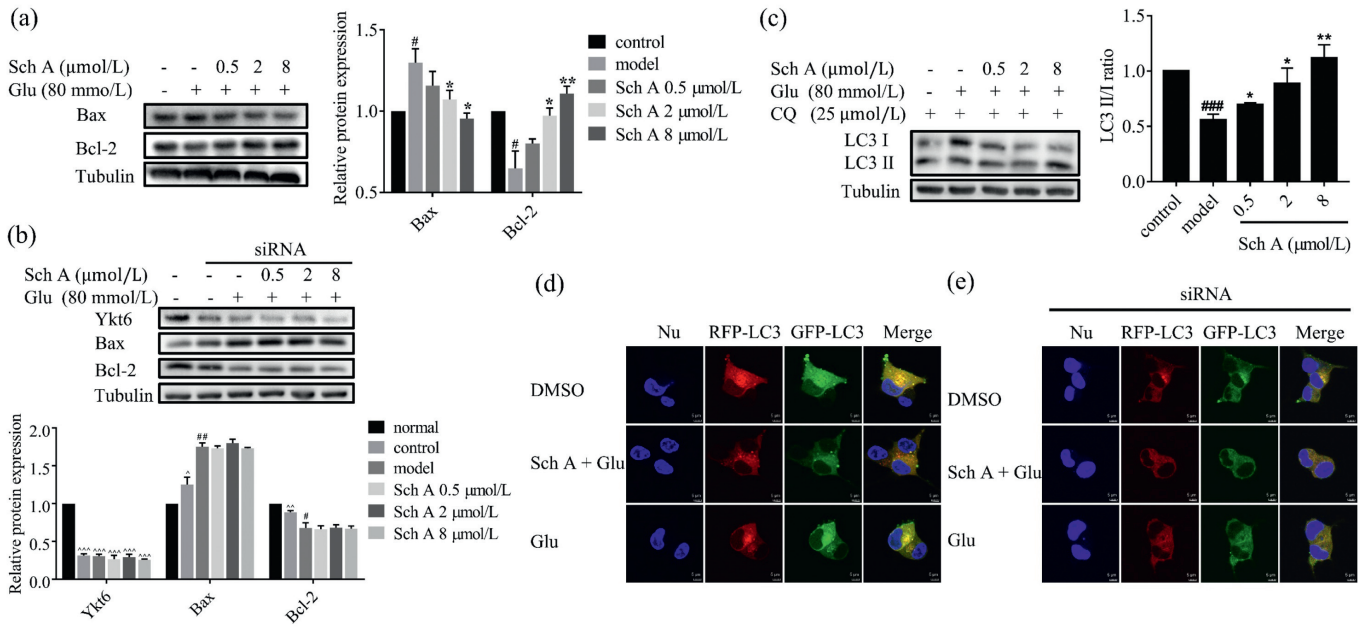

Fig. 4. Sch A exerts the neuroprotective effect by regulating autophagy through Ykt6. (a, b) Bax and Bcl-2 expression levels both in normal (a) or Ykt6 knock-down (b) SH-SY5Y cells induced by glutamate (80 mmol/L) with or without Sch A detected by Western blotting. (c) LC3 I and LC3 II expression levels in SH-SY5Y cells induced by glutamate (80 mmol/L) with or without Sch A detected by Western blotting. CQ = chloroquine. Data are presented as mean ± SEM, $n = 3$ biological replicates per group. Compared with control group: $^{\#}P < 0.05$, $^{\#\#}P < 0.01$, $^{\#\#\#}P < 0.001$; compared with model group: $^{*}P < 0.05$, $^{**}P < 0.01$; compared with normal group: $^{\wedge}P < 0.05$, $^{\wedge\wedge}P < 0.01$, $^{\wedge\wedge\wedge}P < 0.001$. (d, e) SH-SY5Y cells were infected with an RFP-GFP-LC3 expressing adenovirus. Autophagic flux both in normal (d) or Ykt6 knock-down (e) SH-SY5Y cells induced by glutamate (80 mmol/L) with or without Sch A (8 μmol/L) was detected with live-cell imaging microscopy. Scale bar = 5 μm.

of the results even though LC3 could reflect the autophagy level. So, to further judge the extent of autophagy, we measured autophagic flux utilizing an RFP-GFP-LC3 expressing adenovirus to infect SH-SY5Y cells based on the concept of lysosomal quenching of GFP. As a result, a live-cell confocal imaging showed that most of the red and green spots of RFP-GFP-LC3 overlapped in the DMSO group, and nearly all red and green spots overlapped in the Glu group, while the red spots increased after Sch A pretreatment, indicating autophagy enhanced by Sch A (Fig. 4d). Following, we knocked down Ykt6 in the RFP-GFP-LC3 infected cells, and RFP-GFP-LC3 was almost detected as yellow speckles in the merge of all groups, the result indicated Sch A lost its ability to regulate autophagy (Fig. 4e). In summary, Sch A plays a neuroprotective role by regulating autophagy through Ykt6. However, the mechanism of how Sch A interacts with Ykt6 to regulate autophagy is ambiguous. Sch A may drive autophagosome-lysosome fusion or facilitate lysosomal maturation or enhance lysosomal function. This would be the future work to ultimately provide an answer for this mystery.

In this study, we designed and synthesized a variety of clickable probes based on the SAR of Sch A, and obtained active photoaffinity probe **P2**. Through the MS-based pull-down experiment, we identified a series of potential targets of Sch A. In view of Ykt6 being highly reliable and closely related to autophagy and neuroprotection, we further confirmed that Ykt6 was the direct target of Sch A by CESTA, immunofluorescent experiment and the knock-down assay by siRNA. This is also the first reported small molecule regulator of Ykt6 with the KD for 14.6 μmol/L. Furthermore, Sch A played a neuroprotective role by enhancing autophagy through interacting with Ykt6. These results deepen our understanding of the relationship between Sch A and neuronal cell damage-mediated diseases and may provide a potential target for neuroprotective therapy.

Declaration of competing interest

The authors declare that they have no known competing financial interests or personal relationships that could have appeared to influence the work reported in this paper.

Acknowledgments

This work was supported by the CAMS Innovation Fund for Medical Sciences (CIFMS, Nos. 2021-I2M-1-069, 2022-12M-2-002); Beijing Municipal Natural Science Foundation, China (No. 7222259).

Supplementary materials

Supplementary material associated with this article can be found, in the online version, at doi:10.1016/j.cclet.2022.107887.

References

[1] Y. Zhou, L.H. Men, Y.X. Sun, et al., Eur. J. Pharmacol. 892 (2021) 173796.
[2] F.J. Song, K.W. Zeng, L.X. Liao, et al., PLoS One 11 (2016) e0149991.
[3] D.F. Kong, D.Z. Zhang, X.Q. Chu, et al., Biomed. Pharmacother. 99 (2018) 176–183.
[4] K. Sowndhararajan, P. Deepa, M. Kim, et al., Biomed. Pharmacother. 97 (2018) 958–968.
[5] Q. E, M. Tang, X.C. Zhang, et al., Cell. Biol. Int. 39 (2015) 1418–1424.
[6] Y.H. Zhi, Y.X. Jin, L.L. Pan, et al., Arch. Pharm. Res. 42 (2019) 1012–1020.
[7] Q. Wang, L. Liu, H.B. Guan, et al., Pharm. Biol. 59 (2021) 858–865.
[8] S.R. Kim, M.K. Lee, K.A. Koo, et al., J. Neurosci. Res. 76 (2004) 397–405.
[9] B.C. Chen, S.L. Tu, B.A. Zheng, et al., Biosci. Rep. 40 (2020) BSR20200203.
[10] S.C. Fan, C.H. Liu, Y.I. Jiang, et al., J. Ethnopharmacol. 245 (2019) 112103.
[11] C.P. Wang, G.C. Li, Y.W. Shi, et al., J. Physiol. Biochem. 70 (2014) 735–747.
[12] B.J. Chi, Y.S. Sun, J.T. Zhao, et al., J. Immunol. Res. 2022 (2022) 3079823.
[13] Y. Liu, M.P. Patricelli, B.F. Cravatt, Proc. Natl. Acad. Sci. U. S. A. 96 (1999) 14694–14699.
[14] P. Luo, D. Liu, Q. Zhang, et al., Acta Pharm. Sin. B 12 (2022) 2300–2314.
[15] Y. Hu, J. Li, P. Liu, et al., J. Biomed. Biotechnol. 2012 (2012) 728342.
[16] M. Gao, W.C. Zhang, Q.S. Liu, et al., Eur. J. Pharmacol. 591 (2008) 73–79.

[17] J. Slanina, G. Páchniková, M. Čarnecká, et al., J. Nat. Prod. 77 (2014) 2255–2263.
[18] Y.F. Gu, T.Y. Wang, M. Gao, et al., Chin. Chem. Lett. 32 (2021) 380–384.
[19] J. Gnabre, I. Unlu, T. Chang, et al., J. Chromatogr. 878 (2010) 2693–2700.
[20] Y.W. Choi, S. Takamatsu, S.I. Khan, et al., J. Nat. Prod. 69 (2006) 356–359.
[21] X.X. Liang, G.T. Liu, Q.H. Chen, et al., J. Asian Nat. Prod. Res. 12 (2010) 549–556.
[22] D. Hu, N. Han, X.C. Yao, et al., Planta Med. 80 (2014) 671–675.
[23] W. Wang, D.S. Tekcham, M. Yan, et al., Chin. Chem. Lett. 29 (2018) 645–647.
[24] X.R. Yang, Q.X. Xiang, J.R. Xiong, et al., Chin. J. Appl. Chem. 26 (2009) 1070–1074.
[25] S.A. Siddiqi, S. Siddiqi, J. Mahan, et al., J. Biol. Chem. 281 (2006) 20974–20982.
[26] R. Shirakawa, S. Goto-Ito, K. Goto, et al., EMBO J. 39 (2020) e104120.
[27] U. Nair, D.J. Klionsky, Autophagy 7 (2011) 1570–1572.
[28] T. Matsui, P.D. Jiang, S. Nakano, et al., J. Cell Biol. 217 (2018) 2633–2645.
[29] X.Y. Tian, J.L. Teng, J.G. Chen, Autophagy 17 (2021) 2680–2688.
[30] S. Takáts, G. Glatz, G. Szenci, et al., PLoS Genet. 14 (2018) e1007359.
[31] L.K. Cuddy, W.Y. Wani, M.L. Morella, et al., Neuron 104 (2019) 869–884.
[32] H.Y. Li, X. Li, Z.M. Xu, et al., J. Neurosci. Res. 42 (2022) 5641–5654.
[33] J. Dancourt, T.J. Melia, Autophagy 10 (2014) 1470–1471.